Journal of Materials Chemistry A

Accepted Manuscript

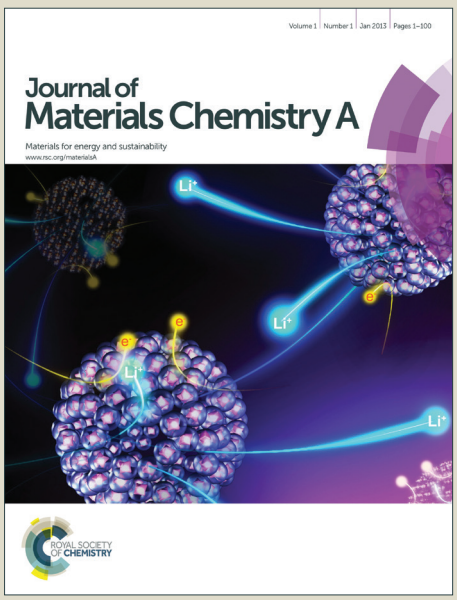

ROYAL SOCIETY OF CHEMISTRY

www.rsc.org/materialsA

Highly-reactive AgPt nanoferns composed of {001}-faceted nanopyramidal spikes for enhanced-heterogeneous photocatalysis application

Akrajas Ali Umar[*a], Elvy Rahmi[a], Aamna Balouch[a], Mohd Yusri Abd Rahman[a], Muhamad Mat Salleh[a], and Munetaka Oyama[b]

[a] *Institute of Microengineering and Nanoelectronics (IMEN), Universiti Kebangsaan Malaysia, 43600 Bangi, Selangor, Malaysia.*

[b]Department of Material Chemistry, Graduate School of Engineering, Kyoto University, Nishikyo-ku, Kyoto, 615-8520, Japan

** Corresponding author Tel.: +603 89118547; fax: +603 89250439*

E-mail address: akrajas@ukm.edu.my *(A.A. Umar)*

Abstract

The structure and property of the catalyst surface determine the physico-chemical process and the reactivity at the surface, such as catalysis behavior, adsorption, surface segregation and charge transfer, etc. The catalyst with surface containing high-energy facet, highly defect or high-energy sites, such as twinning, vertexes, spikes, etc., may facilitate enhanced catalytic and surface reactivity. Here, we present a straightforward approach to synthesize novel nanopyramidal spike composed nanofern of AgPt bimetals vertically-oriented on the substrate surface for potential application in catalysis. High-resolution transmission electron microscopy analysis reveals that the nanopyramidal is characterized by {001} faces, the high-energy facet of *fcc* metal system, promising enhanced catalytic reaction. Crystal growth analysis result determines that a lattice-mismatching effect between Ag and Pt is the key factor for the formation of nanopyramidal AgPt structure and the nanofern suprastructure is produced via an oriented-attachment of the nanopyramidals. The heterogeneous catalytic properties characterisation of AgPt nanofern in the photodegradation of methyl orange in the absence of any reducing agent revealed that the catalytic efficiency is determined by the Ag concentration in the nanocrystals and the morphology of the nanofern structure.

1. Introduction

The preparation of mono-metallic or bi-metallic nanostructure catalyst with high surface reactivity is demanded in many organic reaction applications, including Suzuki, Heck, Stille or Sonogashira, hydrogenation and hydroxylation reactions[1-6]. The syntheses of nanostructures with shape containing high-energy sites, such as surface defect, have become the focus of attention for achieving enhanced-catalytic properties. The results, wide range of shapes of metals nanostructure, ranging from mono and bi-metal system, such as cube, plate, platonic, wires, etc., has been successfully synthesized and enhanced performance in applications have also been demonstrated[7].

Bimetallic nanoparticles has been the concern of many researchers for catalysis applications due to their exceptional physicochemical properties that are always superior over its monometallic nanostructures counterparts[8]. Pt-based bimetallic nanoparticle is amongst the most researched intermetallic compounds so far, thank to its excellent physicochemical properties of individual Pt in variety of organic reactions. So far, several Pt-based bimetallic nanostructures have been prepared and peculiar catalytic properties in wide range of application have been discovered. For example, AuPt [9] has shown excellent catalytic property, which effectively accelerate the reaction, in direct methanol fuel cells. FePt[10] has also exhibited efficient catalytic function in CO oxidation reaction. Several others Pt-based bimetallic nanostructures, such as RuPt[11], PdPt[12], NiPt[13] and RhPt[14], has also shown excellent performance in electrocatalytic oxidation of methanol.

AgPt nanoparticle is amongst the bimetallic system with uniquely high catalytic properties [15, 16] . Intense lattice distortion[17] as well as unique Ag immiscibility[18] in the *fcc* AgPt nanocrystals has been understood as the key driving factor for the generation of unique nanostructure and enhanced-surface physico-chemical properties of the nanocrystals. The decreasing in the electron population in the *d*-orbital of Ag that indicated by the shift in the *d*-orbital bonding energy in AgPt system compared to the pristine Ag[19] is known as to contribute to the improvement of the surface reactivity[20]. Therefore, the synthesis of AgPt nanostructure,

especially with morphology containing high-density high-energy site as well as high-energy basal plane should be continuously demonstrated for enhanced-performance in catalysis applications. Unfortunately, owing to their highly different thermodynamic immiscibility and reduction kinetics, they are difficult to be prepared and shape-controlled growth of the nanostructures is limited. Several methods are available to synthesise the AgPt nanostructures. However, co-reduction method under ambient condition[15] or standard Schlenk line approaches under an argon atmosphere [21] and reaction temperature of 700 °C were favored due to its simple process. However, despite the method successfully achieved the AgPt formation, the shape- , size-, and composition control were not achieved.

In this work, we demonstrate a simple approach to synthesize AgPt intermetallic compound nanostructures by liquid phase deposition (LPD) [5] method directly on the indium tin oxide (ITO) substrate in short time (approximately 10 min) at relatively low temperature (40 °C). The morphology of AgPt nanostructure produced is very unique with structure resembling a "fern" plant. An AgPt "nanofern" is constructed by hundreds of nanopyramidal spikes that mutually orient each other forming nanofern superstructure. With the structure containing high-energy site, thanks to the spiky-pyramid component, the nanofern exhibited highly efficient heterogeneous catalytic properties. The methylene orange was used in this study as a model for evaluating the photocatalytic properties of the AgPt nanofern. It was found that the AgPt nanofern may accelerate the degradation of methylene orange under a solar light irradiation with degradation up to 100 % within only 8 min of reaction time. This is equivalent to ToN and ToF (calculated at 4 min of reaction) as high as 616 and 154 min^{-1}, respectively. The *k* value obtained in kinetic analysis shows that the rate of the photocatalytic degradation of MO increases with the increasing of Ag content in the AgPt nanofern. The present photocatalytic degradatione efficiency result is impressively high in the point of view of heterogeneous catalytic reaction. Owing to its unique morphology with high-energy facet, the nanofern should find extensive use in heterogeneous catalysis applications.

2. Experimental

2.1 AgPt nanofern preparation

The AgPt nanofern was prepared using our recently reported method[5], namely a liquid phase deposition method. In the typical process, a clean ITO substrate (Vin Karolla, USA) was simply immersed into a growth solution that contains 1 mM potassium cloroplatinate (IV), 0.2 mM silver (I) nitrate, 10 mM sodium dodecylesulfate and 5.0 mM formic acid for 30 min. During the growth process, the solution was continuously stirred at 400 *rpm* and its temperature was controlled at 40 °C. After that, the sample was taken out from the solution and rinsed with a copious amount of pure water. The sample was then finally dried with a flow of nitrogen gas.

All the chemicals were purchased from Fluka and used directly without any further purification process and in the nanostructure growth preparation, their solution were prepared in aqueous system that was obtained from Milli-Q water purification system with quality as high as 18.2 MΩ • cm at 25 ° C.

In the typical synthesis process, the color of the solution gradually changed from light yellow to transparent with time. Using this approach, the AgPt nanostructure can be grown on the ITO surface as well as on the walls of the vial glass. Uniform black film will be obtained on the substrate surface everytime completing the growth process.

The morphology of the AgPt nanofern was characterized by high-resolution transmission electron Microscope (TEM) and the field emission scanning electron microscopy (FESEM) using JEOL JEM-ARM200F operated at 200 kV with resolution of 0.8 Å and Zeiss Supra 55VP FESEM model with resolution of 1.0 nm at 30 kV, respectively. The structure and composition were verified by EDX elemental mapping, X-ray photoelectron spectroscopy (XPS) and X-ray diffraction (XRD). The EDX elemental mapping was obtained from the FESEM apparatur equipped with the EDX analysis tool. The XPS analysis was carried out using Bruker XPS apparatus XSAM-HS from KRATOS, UK with monoenergetic soft X-ray Mg K α (1253.6 eV) or Al K α (1486.6 eV) irradiation and Omni Focus III input lens to analyser. The XRD analysis was carried using Bruker D8 system with a CuKα irradiation and a scanning rate of 0.025°/s. Reflection geometry was used during the XRD analysis.

2.2 Heterogeneous photocatalytic characterization

The catalytic property of the AgPt nanofern was evaluated in the photocatalytic degradation of methyl orange. In the typical process, AgPt nanofern modified ITO substrate was immersed into 10 mL of 20 mg L^{-1} aqueous solution of methyl orange solution. The reaction was then irradiated with a solar light spectrum obtained from low-cost solar simulator (AM1.5, 100 mW cm^{-2}). The photocatalytic effect of AgPt nanofern catalyst was evaluated by recording the absorption spectrum of the methyl orange solution, by taking approximately 3 mL of the reaction every 2 min, using a Perkin-Elmer Lambda 900 UV-visible-NIR spectrophotometer. The photocatalytic efficiency of the AgPt nanofern was calculated based on both the mole and the active surface area of the catalyst. The degradation of MO under light irradiation in the absence of AgPt nanofern and under dark in the presence of AgPt nanofern were also experimented to further verify the role of AgPt nanofern in the degradation of MO.

The BET analysis was carried out using Micrometic 2020 apparatus. Prior to adsorption and desorption analysis, the sample was degassed at 300 °C for 10 h to remove any organic compound on the surface. The weight of the sample after degassed was recorded. Adsorption and desorption experiment was carried out using nitrogen gas at -196 °C. AgPt nanofern on ITO slide with total weight of 1 g (AgPt nanofern + substrate) was used in this experiment.

In this study, we discovered that the ITO substrate had no contribution to the adsorption and desorption of N_2 gas so that the obtained-surface area can be directly associated with the AgPt nanofern. In typical procedure, the BET surface area was found as high as 51.6 $m^2 g^{-1}$. By considering the mass of AgPt nanofern on a single ITO slide of as high as 34 μg, the specific surface area of AgPT nanofern on a single ITO slide is 0.00176 m^2.

In order to obtain the final concentration of MO after the photocatalytic degradation reaction, optical absorption calibration standard was recorded. In this case, MO with eight different concentration from 1-35 mg L-1 were used and the optical absorption spectrum of each concentration is recorded. The calibration curve was obtained by extrapolating the absorbance value at the absorption peak of MO at 465 nm with their corresponding concentration. A straight-line of $y = mx + C$ with R^2 as high as 0.99 was obtained via a linear regression analysis, in which

y, *m*, *x*, and *C* are absorbance at the centre band, slope of the graph, concentration and intersection point with *y*-axis, respectively. The typical calibration data for the optical absorption of methyl orange observed, is shown in Figure S1 (Supporting Information).

3. Results and Discussion

3.1 AgPt nanofern synthesis and characterization

A shinny black color was observed on the ITO substrate after an immersion for 30 min at 40 C into the growth solution containing K_2PtCl_6, Ag NO_3, sodium dedecyl sulfate (SDS) and formic acid. The phase of the nanostructure that formed on the surface of ITO substate was analyzed using X-ray Diffraction (XRD). The result is shown in Figure 1. As Figure 1 reveals, three prominent peaks that can be related to the existence of AgPt bimetal system are exist in the spectrum, i.e. at $2\theta = 39.854°$, 46.3° and 67.6°. Others peaks are attributed to the ITO substrate. These three peaks were found to closely match, but slightly shifted; with the diffraction from (111), (200) and (220) Bragg planes of Pt, respectively, inferring an effective formation of intermetalic compound system upon introduction of Ag ions into Pt host lattice[22]. Insert table in Figure 1 shows the comparison between the diffraction peaks position of AgPt bimetal and individual Ag and Pt. As can be seen from the table, the AgPt peaks positions for main lattice planes are shifted to the lower angle respected to the individual Pt for about 0.11 to 0.27° and Ag (for about 0.31 to 0.75°) except for (200) plane, which is above Ag). Actually, the AgPt bimetal system does not fit to conventional *fcc* lattice, such as Ag and Pt. Therefore, the incorporation of Ag into Pt may not adopt the symmetry of one of or combination of these two components or unit length in between the two systems[21]. As has been reported in literature, at particularly high-concentration of Ag, lattice distortion is very extensive affecting both inter-atomic distances on the surface lattice plane and d-spacing of neighboring lattice plane[17]. Because of the anisotropy property of the stress produced upon the introduction of Ag ion into the lattice, the nature of distortion, including d-spacing shifting, inter-atomic distance change, etc., will differ from one

lattice plane to another plane[23]. Thus, the difference in the tendency of lattice planes shifting is expected in this case.

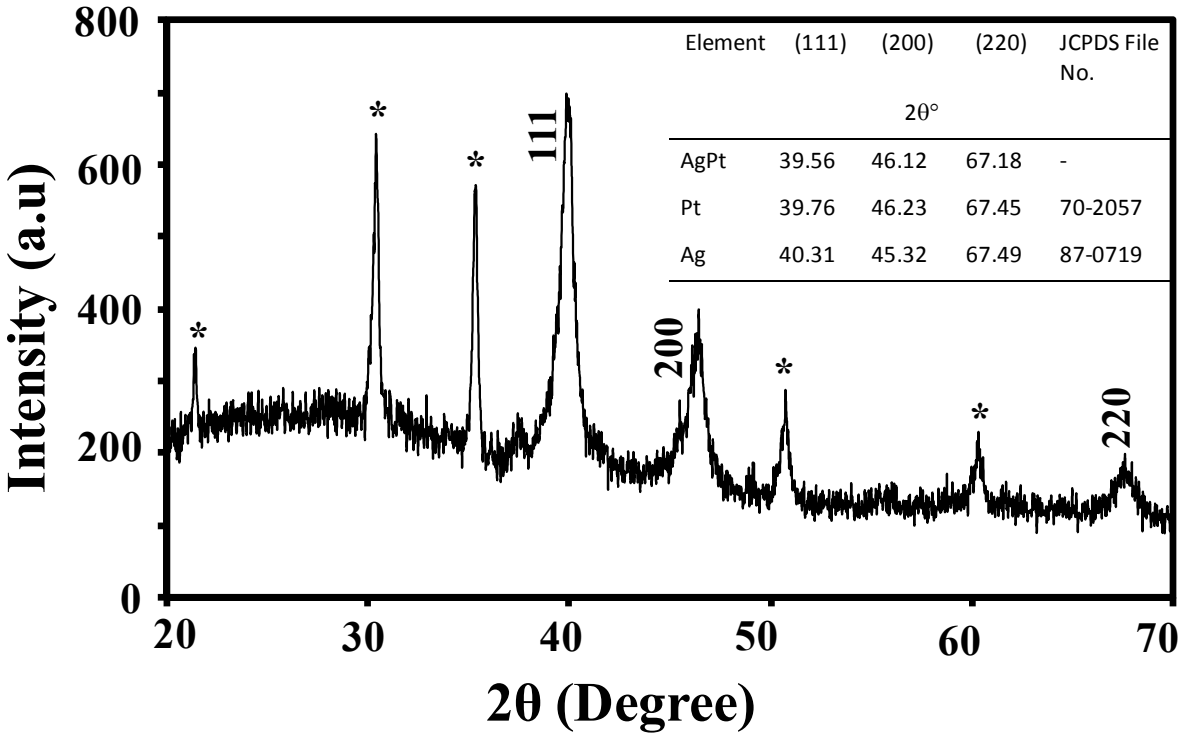

Element	(111)	(200)	(220)	JCPDS File No.
		2θ°		
AgPt	39.56	46.12	67.18	-
Pt	39.76	46.23	67.45	70-2057
Ag	40.31	45.32	67.49	87-0719

Figure 1. The XRD patern of AgPt nanofern.

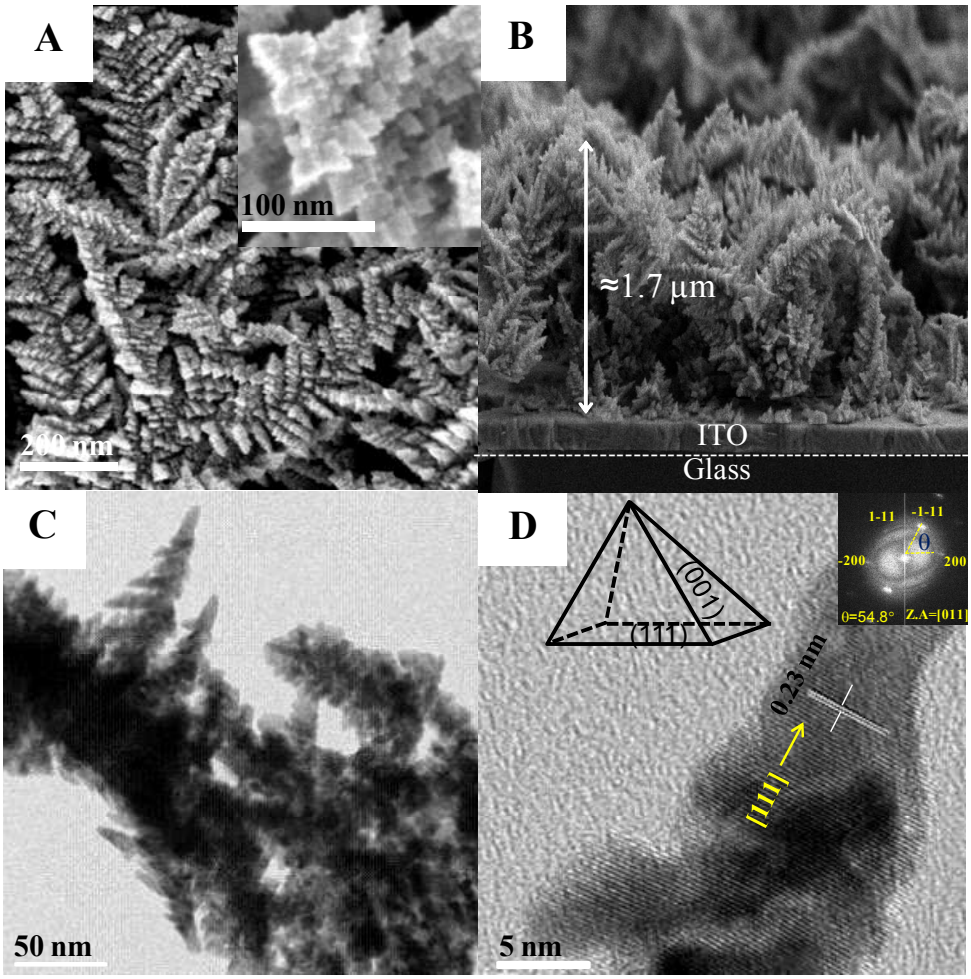

Figure 2. (A) FESEM image of AgPt nanofern prepared using a growth solution that contains 1 mM potassium cloroplatinate (IV), 0.2 mM silver (I) nitrate, 10 mM sodium dodecylesulfate and 5.0 mM formic acid with growth time for 30 min. Inset in A is the high-resolution of the AgPt nanofern peak. (B) Cross-section view of the nanofern. (C-D) Low and high-resolution TEM image of AgPt nanofern. Insets in D are the geometry of the nanopyramid that composes the nanofern and the Fourier transformed -lattice fringe image.

Figure 2 shows typical morphology of AgPt nanostructures grown on an ITO substrate. As can be seen from the Figure 2A, the AgPt exhibit a unique morphology resembling ferns structure vertically grown on ITO substrate. The "nanofern" growth, judging from the FESEM analysis, covers almost 85% of the ITO surface. The nanofern are constructed by overlapping and mutual oriented of hundreds of sharp-vertices (spike) and rugged-surfaced-nanopyramid structures. The nanopyramid size (i.e. edge-length) ranges from 9 to 14 nm. Cross-sectional analysis on the structure found that the nanofern's height can be from 500 nm up to 1.7 um (see

Figure 2B). Considering the morphology of the nanofern that is constructed by dozens of branches on each stalk with their peculiar nanopyramid component, the AgPt nanofern may be highly reactive the result of its high surface area and high-energy atomic sites. Thus, it has a great potential for accelerating the organic reactions.

A HRTEM analysis was carried out to investigate the bulk crystallinity of the nanofern. The result is presented in Figure 2D. The result presented here was imaged from zone axis of [011]. The selected-area electron diffraction obtained in this work agrees with the recently reported result, [24] confirming the bi-metalisation of the system. Interestingly, in contrast to its morphology that is constructed by the nanopyramid with a rugged-surfaced- structure as well as the nature of their mutual orientation to form the nanofern, the nanofern is single crystalline in nature. It is indicated by the absence of twinning or dislocation in the lattice fringes. This inferred that the nanopyramid attached in well-orientation each other to form bigger nanofern structure. Analysis on the fringe spacing, it was found that the *d*-spacing is approximately 0.23 nm (see Figure 2D), which is belong to (111) plane. Therefore, the nanofern grow toward the [111] direction. Considering the symmetry of the nanopyramid with a square base, the four congruent isosceles triangles faces should be belong to {001} Bragg plane (see inset in Figure 2D). Nevertheless, the atoms at the nanopyramid edge should be belong to the {110} planes, the highest energy surface in *fcc* metal system. Thus, the AgPt nanofern feature a high energy structure. It may be potential for catalysis application.

Significant shifting in the XRD pattern from individual Pt has actually revealed the successfulness of Ag and Pt intermetallic compound formation. To further verify the formation of AgPt bimetal system, EDX analysis was carried out. Several positions on the sample surface were chosen for this purpose. The result is shown in Figure S2 (Supporting Information). It is found that both elemental Ag and Pt are present with atomic weight percentage as high as 9.54% and 90.46%, for Ag and Pt respectively. This result is in agreement with the XRD data, confirming the successful formation of AgPt bimetal system.

While the EDX analysis confirms the formation of AgPt bimetal, the X-ray Photoelectron Spectrocopy (XPS) analysis was performed to determine the valence state and the surface composition of the AgPt nanofern. The result is shown in Figure 3. Shirley-type background was used in the curve fitting process with Gaussian-Lorentzian (G-L) mixed function (70% Gaussian and 30 % Lorentzian components) as the peak line shape. C1s binding energy of 285 eV was used as the calibration curve for all the core level spectra. Figure 3b-c shows the typical high resolution spectra for Ag (3*d*) and Pt(4*f*) core level states.

On the Pt (see Figure 3B), based on the three spin orbit pairs appears on Pt $4f_{7/2}$ curve as obtained from the Gaussian-Lorentzian fitting, its chemical state is simply composed of two oxidation states, namely Pt^0 for 71.37 eV (curve 1) and two Pt^{2+} at 71.90 (curve 2) and 72.99 (curve 3) eV. This reveals that the Pt characteristic in the intermetallic compound system is on a reduced state from Pt^{4+} to Pt^{2+} and Pt^0 species. When Pt $4f_{7/2}$ binding energy of AgPt nanofern is compared to the pure Pt, i.e. 71.3 eV, the binding energy shows a positive shift, inferring the AgPt highly active surface property. This nature seems to be further validated as the fact of higher intensity of Pt^{2+} than the Pt metallic state (Pt^0). Meanwhile on the Ag, its $3d_{5/2}$ spectra might be composed of a double spin orbit, namely at energy of 367.95eV and 369.19eV. However, due to its low intensity and the contribution of high-noise level, the peak at 369.19 eV can be simply neglected. Thus, this infers that the Ag is available in the metalic state only. If energy level of Ag $3d_{5/2}$ compared to pure Ag system (368.27 eV), its binding energy shows a negative shift (to lower energy level), indicating the occurrence of effective electron transfer from Ag to Pt. This should be valid as the Ag features an electron donating property, while the Pt itself has *f* orbital that has more than half filled, enabling electron accepting from the Ag for bimetal formation.

It was found that the molar ratio of Ag and Pt on the surface is approximately as high as 1:10. This result is consistent with the bulk elemental analysis using EDX in which the elemental composition of Ag and Pt in AgPt bimetal nanofern is 9.54% and 90.46% respectively. Considering the Pt is dominant in the compound with high-density Pt^{2+} state as well as

significantly high positive energy shifting, the AgPt nanofern promises highly-catalytic properties.

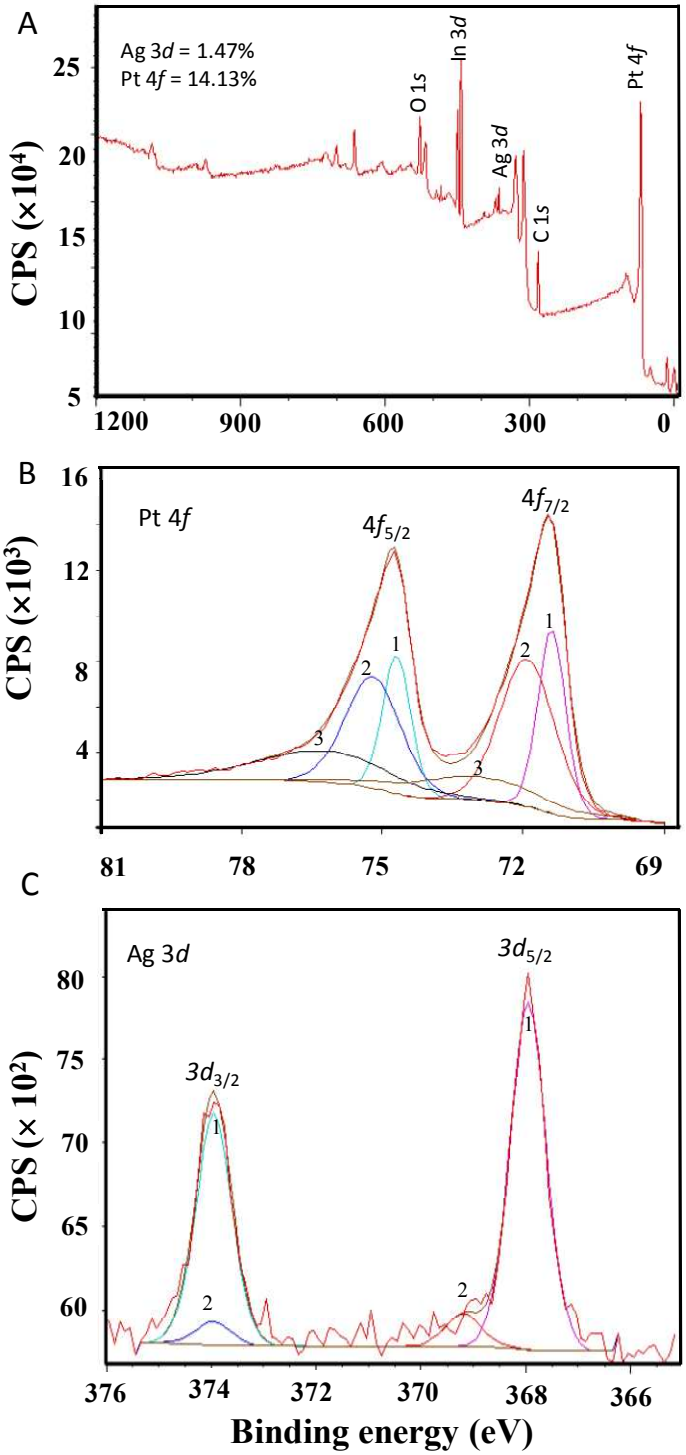

Figure 3. (A). Wide-spectrum scan of AgPt nanofern grown on ITO substrate surface. High-resolution spectra for Pt 4*f* (B)and Ag 3*d* (C). The Pt $4f_{7/2}$ consist of three pairs overlapping

Gaussian-Lorentzian curves, which is associated with Pt^0 (1) and two Pt^{2+} (2 and 3). Meanwhile Ag $3d_{5/2}$ composed of 1 dominant curve, related to Ag^0. Curve 2 is neglected due to its low-intensity.

At the moment, the mechanism of the formation of AgPt nanofern is not yet clear. However, the presence of Ag^+ ions in the reaction (from $AgNO_3$) is assumed as the key factor for the formation of nanopyramidal constructed-AgPt nanofern. The following facts are likely the validation on this assumption. The AgPt nanofern is actually prepared using the original recipe for Pt fibrous nanocubes[5] growth that our group developed recently. The original reaction contains Pt precursor ($PtCl_4^{-2}$), sodium dodecyl sulphate as a surfactant and formic acid as a reducing agent. From this reaction, high-density fibrous nanocube of Pt can be realized directly on the substrate surface that was grown at 40 °C. By simply introducing the $AgNO_3$ in the original reaction, novel nanostructure, namely nanopyramid constructed-nanofern, were obtained. No fibrous structure or cubic nanostructures were obtained from this new reaction system. As have been described in the EDX and XPS analysis, the nanofern are the AgPt intermetallic compound. On this basis, we hypothesize that the nanofern formation could be as the effect of the lattice-mismatch induced crystal growth[25]. As has been well-known, the lattice mismatch between Ag and Pt is as high as 1%. Such difference in the lattice constant has promoted the formation of square-base isosceles nanopyramid, instead of spherical morphology. As has been well-known, the metal nanostructure morphology can be modified by the addition of a trace amount of other ions in the reaction. In this case, the Ag ion presence in the reaction may affect the Galvanic-assisted reduction and binding selectivity to the Pt system in which then it could restrict or increase the crystallographic growth rate toward particular direction in the nanocrystal[17, 19, 26].

As also described earlier, the basal plane of the nanopyramid is (001), one of the highest surface energy of *fcc* metal system. In the effort of surface energy minimalization[27], the nanopyramid are mutually attached each other and re-oriented to form nanofern morphology.

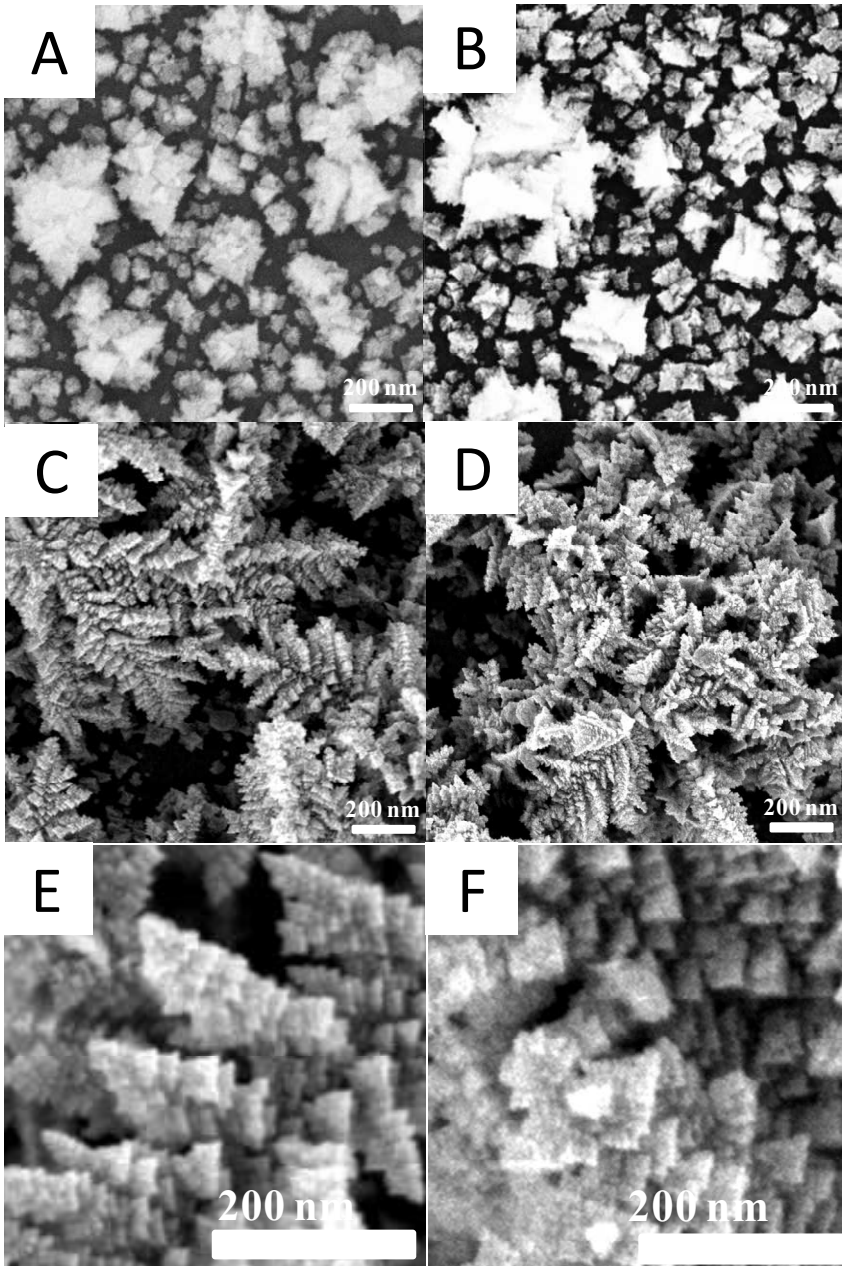

Figure 4. AgPt nanostructures prepared using different Ag ions concentration, namely 0.07 (A), 0.13 (B), 0. 20 (C) and 0. 30 mM (D). F is high-resolution image of D showing distorted-structure of nanofern, while E is high-resolution image of C for comparison. The concentration of others reactant are fixed at the condition as shown in Figure 2.

Lattice-mismatch effect on the nanofern crystal growth was likely further verified when enhanced nanofern formation on the surface when the concentration of Ag^+ ions increase from 0.066 to 0.2 mM in the reaction and become distorted when relatively high Ag^+ ions concentration (0.3 mM) was used in the reaction. The result is shown in Figure 4. In order to

confirm the increasing of Ag concentration affects the Ag substitution in the Pt host nanocrystals, energy-dispersive X-ray spectroscopy was carried out on the samples of AgPt nanofern prepared using several Ag concentrations. It was found that the increasing of Ag concentration causes the increase in the Ag and Pt atomic ratio in the nanocrystals. For example, the Ag and Pt ratio as low as 1:37 was obtained if the AgPt nanofern prepared using Ag concentration of 0.006 mM. The ratio successfully increases to 1:6 if using Ag concentration of 0.33 mM. The optimum sample has the Ag : Pt ratio as high as 1:10. The EDX spectra as well as the atomic ratio of Ag and Pt are shown in Figure S3 (Supporting Information). Based on these result, it can be confirmed that the effect of Ag substitution into the Pt lattice may has induced structural growth orientation in the fcc Pt system, namely to highly anisotropic morphology of nanofern or distorted nanofern if using relatively high Ag concentration. In addition to this interesting phenomenon, this result also reveals that the atomic ratio between Ag and Pt in the AgPt nanofern is possible to be controlled. Therefore, beside the modification on the morphology, novel properties are expected to be produced from the bimetallic system when the atomic ratio of Ag and Pt is varied.

Despite the Ag^+ ions has been recognized as the key factor for the formation of nanofern structure, we also evaluated the extent effect of other reactants, such as formic acid reducing agent and SDS surfactant, on the nanocrystal growth. The Ag^+ ions and Pt precursor concentrations were kept unchanged at the optimum condition. For the case of formic acid, it was found that augmenting the formic acid concentration increases the density of the nanofern formation on the substrate surface. It is noted that the concentration that allows the formation of AgPt nanofern is in the range of 3 to 10 mM and it is optimum at 5 mM (the condition for the preparation of AgPt nanofern as shown in Figure 1). Low-density of irregular shape nanostructure or no nanocrystal growth were obtained if the concentration is lower than 0.3 mM. Meanwhile, a low-density distorted nanofern was obtained if the concentration is higher than the optimum concentration. As has been well-known, the optimum activation of a particular surface molecule of $AgNO_3$ and K_2PtCl_6 by reduction agent is required in the process of formation of bimetal nanoparticles. If formic acid concentration is low or high, the nanofern structure is improperly formed. The results are shown in Figure S4 (Supporting Information).

Regarding the SDS surfactant, their presences exhibit a key factor for branching formation influence[28], thus influence the symmetry of the nanofern structure. The sample that is shown in Figure 1 was prepared using SDS concentration of as high as 10 mM. As has been mentioned, at this condition, nanofern with well-symmetry of spiky nanopyramid were obtained. The increase in the concentration of SDS from the optimum condition, for example to 15 mM, induces active branching in the nanofern structure, producing distorted nanofern. However, if such condition is used in the application, the SDS concentration can be used for the preparation of AgPt nanofern. Vice versa, for the case of concentration is lower than the optimum condition, less branched-nanofern is produced. The results are shown in Figure S5 (Supporting Information).

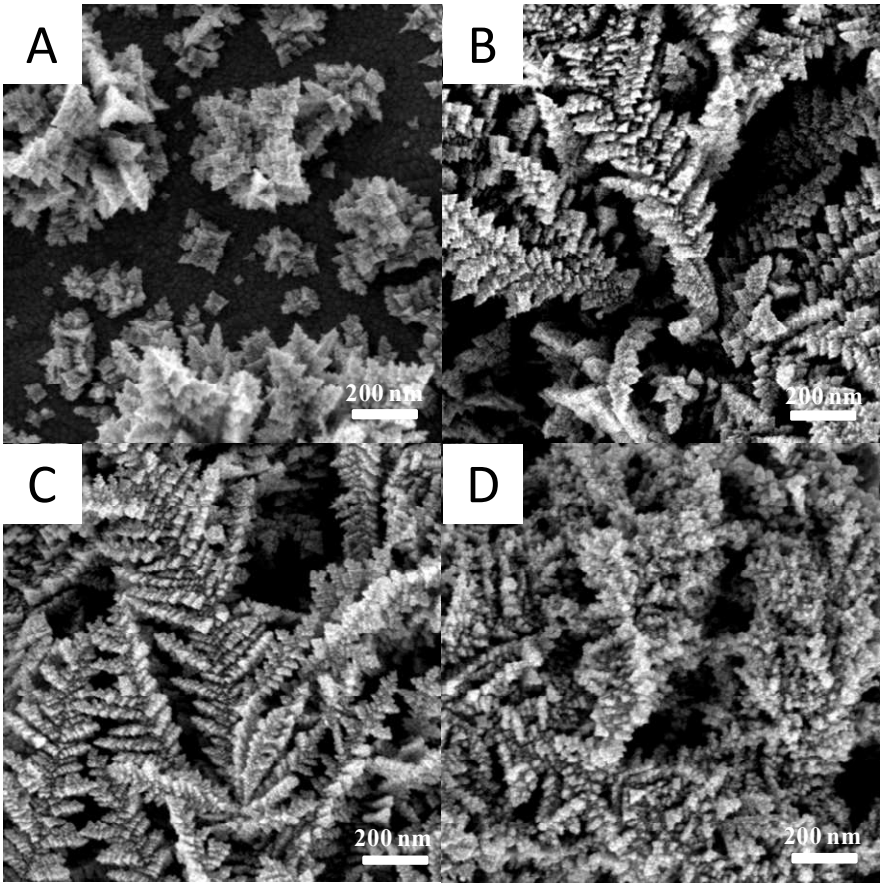

Figure 5. AgPt nanostructures prepared at different growth temperatures, namely 30 (A), 40 (B), 60 (C) and 80 °C (D). The growth solution is the optimum condition as used in Figure 2.

Finally, temperature is also found to have a certain unique role in the formation of nanofern structure. In the optimum condition, the nanofern synthesis was performed at 40 ^{o}C. High-density nanofern with well-symmetry can be grown on the substrate surface. If lower temperatures is applied (i.e. 30 °C), smaller size nanofern that is composed of sharp-spike-nanopyramid was obtained. Unfortunately, the nanofern density is lower than the optimum condition. Meanwhile, for temperature higher than the optimum one, for example 50 °C, despite the density as well as the nanofern size is relatively unchanged compared to the optimum condition, the nanopyramid component size decreases with the increasing of temperature. It is due to the supersaturation of nanoparticle formation that leads to the formation of smaller size nanostructure (16). Moreover, the vertices of the nanopyramid component become more rounded with the increasing of the temperature. At a relatively high growth temperature, i.e. 80 C, truncated or damaged nanofern is obtained. The result is shown in Figure 5.

3.2 Heterogeneous photocatalytic characterisation.

Figure 6 shows typical dynamic optical absorbance of methyl orange (MO) during the photocatalytic degradation in the presence of single slide of ITO containing AgPt nanofern. As the Figure 6A reveals, the optical absorbance of MO at the main absorption band (centering at 465 nm) rapidly decreases with time indicating effective degradation of MO. Its kinetic degradation during the photocatalytic reaction is presented in the inset of Figure 6A. It is shown that, for example, for a reaction time of only for 1 min the concentration of MO decreases as high as approximately 21%. It then almost completely degraded (100% degradation) for a reaction time as short as 8 min. By considering the number of catalytic site or active sites (i.e. the effective sites for adsorption and heterogeneous catalytic reaction) of AgPt nanofern catalyst of as high as 3.27×10^{14}, which was obtained by dividing the specific surface area (i.e. 0.00176 m^2 -obtained from the BET analysis result) of AgPt nanofern catalyst (approximately 34 μg of weight) on a single ITO slide ; with "dynamical diameter" of MO molecules (as high as 2.6×10^{-9} m), the turnover number and turnover frequency of the reaction (calculated at the 4 min of the reaction) are as high as approximately 616 and 154 min^{-1}, respectively (see Figure 6B) (see the supporting information for a detailed calculation of TON and TOF). As also revealed in Figure 6B, the TOF exhibit exponential increase with times, in which an extremely fast reaction was

obtained at the first minute of the reaction with values 224 min^{-1}. However, it exponentially decreased with time to 140 min^{-1} at the reaction time of 8 min. This is an indication of site saturation or deactivation [29-31] on the AgPt surface that hinders further adsorption of adsorbates for further catalytic degradation (Michaelis–Menten kinetics). This phenomenon seemed to be valid, judging from the data obtained from repeated used of AgPt nanofern in multiple photodegradation of MO, in which the kinetic rate of catalytic degradation decreased with the increasing of use-cycle (see Figure 7). Nevertheless, the AgPt still exhibits high-photocataytic property at least for three times repeated use in the reaction. The decreasing in the performance upon repeated-use, especially at higher concentration of analyte than the catalyst, is normal in the catalytic reaction process and it is simply due to the site saturation on the catalyst surface[32, 33], the result of strong analytes bond on the catalyst surface or site poisoning[31, 34]. Because in the present study the catalytic reaction depends on the concentration of the reactant (MO), verified by the reaction kinetic analysis (see Figure 7) that shows the reaction follows a first-order reaction kinetic, in which the $\ln(C_i/C_0)$ linearly related with the reaction time, the site saturation might be managed by using the AgPt nanofern catalyst with concentration comparable with the MO[31]. With this condition, the reactant-product may have appropriate life-time to complete adsorption-desorption process before continuing for subsequent reaction[35]. The use of elevated temperature during the reaction can also be considered[36] as an effective approach to address the site saturation and catalyst regeneration issues as the temperature application may shorten the adsorption-desorption process. Thus, accelerates the reaction. However, relatively high-temperature may deteriorate the morphology of the nanocatalyst.

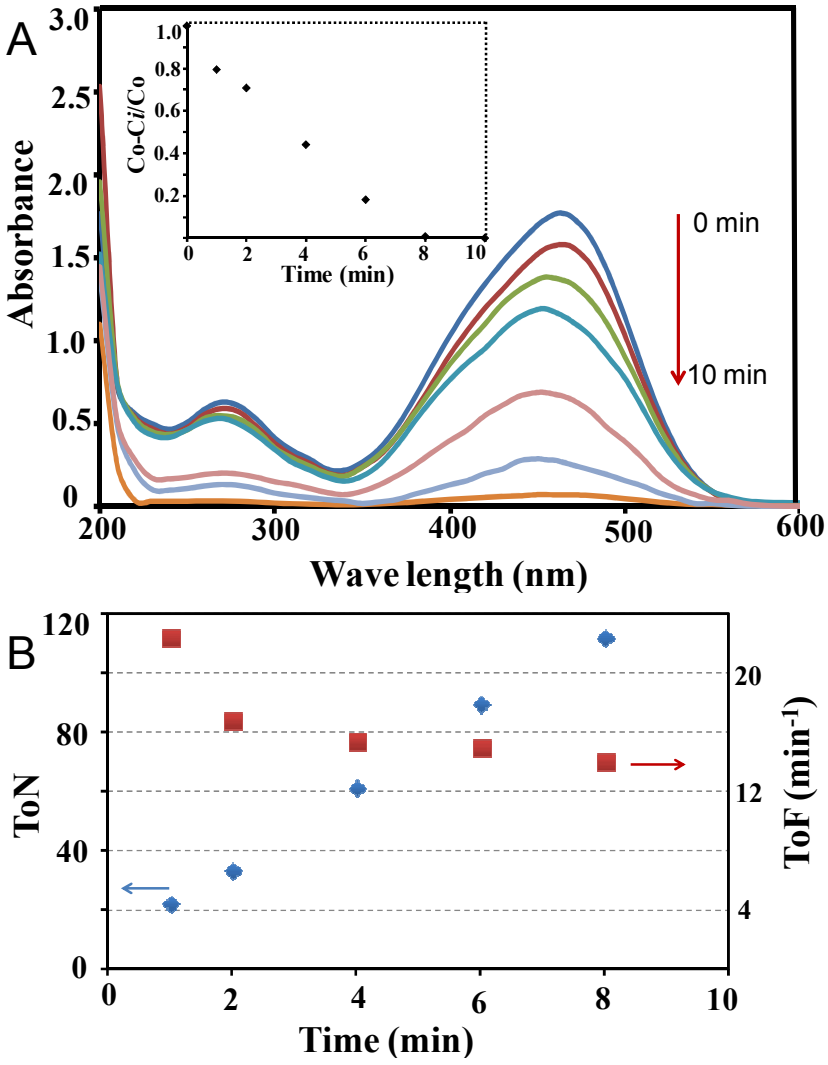

Figure 6. (A) The optical absorbance of 20 ppm MO during the photocatalytic degradation under irradiation of white light source (AM1.5 at 100 W cm^{-2}) and in the presence of one slide of ITO containing AgPt nanofern. Inset in A is the concentration of MO during the reaction. (B) The turnover number (ToN) and turnover frequency (ToF) of the heterogeneous photocatalytic degradation of MO over AgPt nanofern.

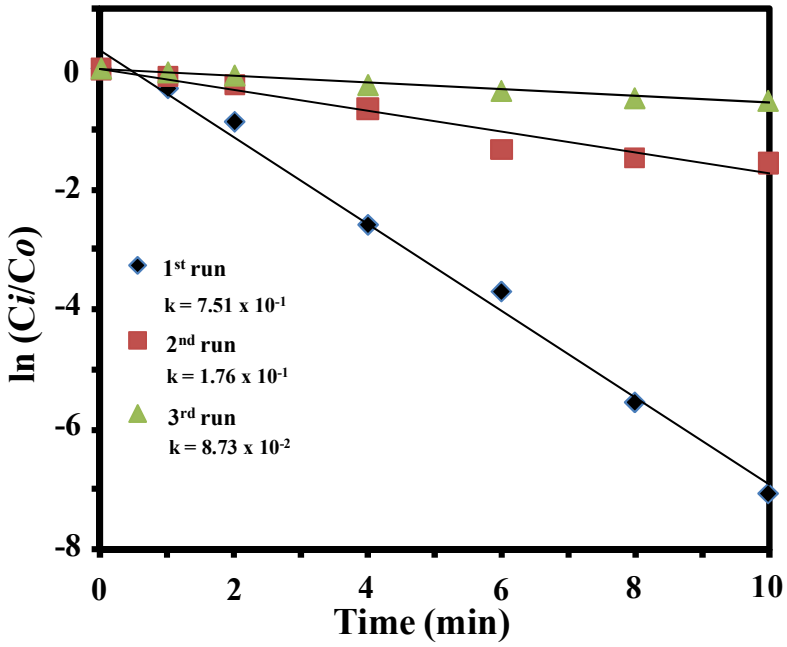

Figure 7. The kinetic rate of MO degradation over multiple-use of single slide AgPt nanofern catalyst.

Table 1. Comparison of Methylene Orange degradation over several types of metal-metaloxides nanocatalyst.

No	Catal. System	Method	Reaction	Rate Constant, *k*	Ref.
1	AgPt	Photocatalytic	Heterogeneous	0.75 min^{-1}	This work
2	Pt-Fe_2O_3	Electrochemical	Heterogeneous	0.42 min^{-1}	[37]
3	Pt@TiO_2	Photocatalytic	Homogeneous	0.08 min^{-1}	[38]
4	Pt-TiO_2	Photocatalytic	Homogeneous	0.11 h^{-1}	[39]
5	Ag-ZnO	Photocatalytic	Homogeneous	0.19 min^{-1}	[40]
6	N/Pd-TiO_2	Photocatalytic	Homogeneous	0.02 min^{-1}	[41]

It can be noted that the present study did not use any reducing agent to accelerate the reduction or degradation of MO as normally used in the photodegradation of MO. Thus, this result is absolutely surprising and much efficient compared to the recently reported result utilizing variety of metallic nanocatalyst and even much efficient if compared to the homogeneous reaction system utilizing Pt-base nanocomposites catalyst[37-39, 41]. Table 1 summarizes the comparison of AgPt nanofern catalytic performance to the recently reported results. This could be due to the following reasons: Firstly, the effect of the high-energy nature of the nanofern structure. As confirmed by the FESEM and HRTEM imaging analysis, the nanofern is composed of nanosized tetrahendron pyramid with four congruent isosceles with rugged-(001) faces (see inset in Figure 2D) facilitating facile surface reaction and analytes adsorption. In addition, the nanopyramid is characterised by sharp and spiky vertices, producing highly reactive sites due to high electron density. In spite of this high-energy nature, no MO degradation was observed when light irradiation was absence, reflecting the unique photocatalytic induced reaction of the system (see Figure S6, Supporting Information). We also examined the photocatalytic degradation efficiency of nanofern if their structure modified to further verify the shape effect in the catalytic property. By preparing the sample at different growth temperature, nanofern with different morphology, from spiky to rounded nanopyramid composed nanofern, were obtained. It was found that the most efficient catalytic reaction occurred on the spiky nanopyramid based-nanofern. The reaction rate then decreased with the increasing of rounded-vertices percentage on the structure, namely from 0.56 min-1 to 0.21 min-1 for the spiky to rounded nanopyramid, respectively. The result is shown in Figure 8.

It has been earlier discussed that the tetrahedral AgPt nanopyramid with (111) basal plane and {001} isosceles should possess {110} atoms at its edges, the highest energy of *fcc* metal, at which the surface reaction is expected to actively occurred. The decreasing of the photocatalytic efficiency upon morphology modification can be directly related to the decreasing of these high-energy surface portions in the nanostructures. As has been revealed in the FESEM image, the nanopyramid is rounded when prepared at an elevated temperature. This infers that not only the {110} atoms at the edge annealed into a more stable lattice plane, i.e. {111} planes but also the

{001} planes. Thus, the surface reactivity is decayed. XRD analysis on the AgPt nanofern prepared at different growth temperature indicated the decreasing of the diffraction intensity of {001} respect to {111}, confirming the modification of dominant lattice plane of the nanostructure (see Figure S7, Supporting Information). The effect of the change in the surface area when prepared at high-temperature on the decreasing of surface activity might be neglected in this case because the surface reaction is determined much by the high-energy site on the surface. Since the high-energy site might have annealed to more stable lattice plane, the change in the surface area might only give little effect on the surface reactivity.

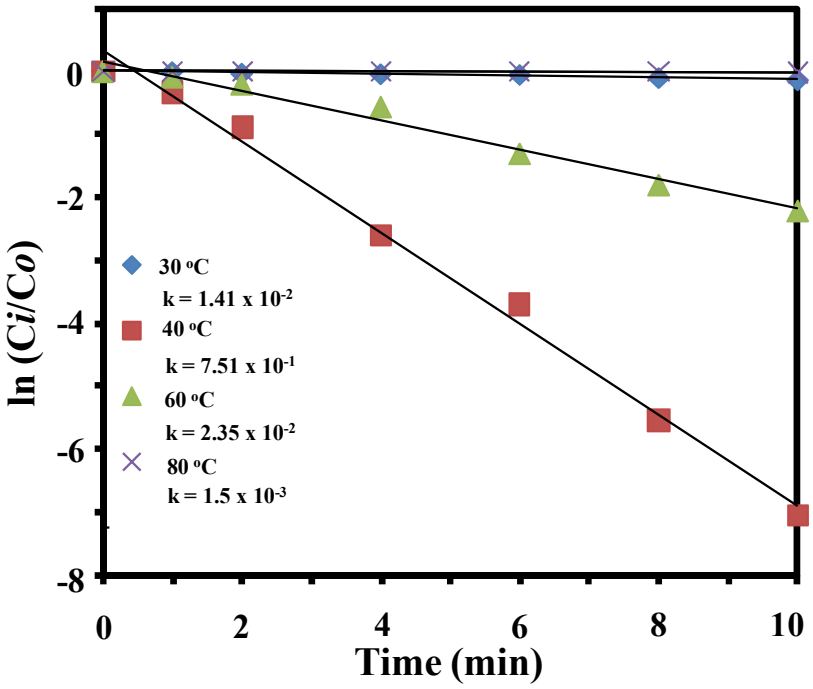

Figure 8. The photodegradation kinetic rate of MO over AgPt nanofern prepared at different growth temperatures.

Secondly, the effect of enhancement of the surface reactivity due to the presence of Ag doping is assumed as another key factor for the high-efficient catalytic properties. It has been well-known that beside the Ag induced lattice distortion in the bimetallic crystal, it also produce

novel properties due to the change in the Ag *d*-orbital electron population, generating highly-reactive surface property because of the decreasing in the stability of electronic level in the bimetallic system[17, 20]. The presence of dominant Pt^{2+} state and significantly high positive shifting in the bonding energy of orbital electronic system upon intermetallic formation process with Ag, as confirmed by the XPS analysis result, adds to the highly-reactive surface properties of AgPt nanofern. In the study of the effect of Ag doping concentration on the catalytic performance of the AgPt nanofern, it was found that the catalytic efficiency increased with the increasing of Ag doping concentration and optimum at the 0.2 mM. TOF as high as 15 min^{-1} was obtained at this condition. No significant improvement was observed when the concentration is further augmented. Figure 9 shows typical kinetic degradation of MO and their kinetic degradation rate analysis under different concentration of Ag in AgPt nanofern catalyst. As the Figure 10 reveals, in good agreement with the ToF value, the kinetic rate significantly improved as the Ag concentration increased in the nanofern. At the optimum Ag doping concentration, the kinetic rate as high as 0.75 min^{-1} was obtained. From the Figure 10, it is true that the k value for the sample with Ag 0.33 mM is the highest. However, this sample showed a lower performance stability due to morphology distortion from the nanofern shape (see Figure 5D). Thus, the sample with Ag concentration of 0.2 mM is the optimum.

The decrease in the performance upon increasing the Ag ion concentration can be related to extreme modification on the nanocrystal morphology due to lattice contraction upon high-concentration Ag substitution. It has been reported that the increase in the Ag concentration in the AgPt system intensify the surface stress[42] and at an extreme case it may cause a decrease in the structural coherence in the nanocrystals[23, 43]. As has been mentioned earlier, the phenomenon can be observed from the increasing of surface plane inter-atomic distance and the decreasing of spacing between the neighboring plane[17]. This may modify both the surface atomic structure and surface electronic properties. Thus, modify the photocatalytic properties. Such effect was also observed in the FePt system[44]. FESEM image in Figure 5D-F clearly indicates such nanocrystal morphology modification under high-concentration Ag substitution, as the presence of low-symmetry nanopyramidal component of the nanofern. An AgPt nanofern with highly stable lattice plane, i.e. {111}, instead of high-energy lattice plane, is expected from the result. We carried out XRD analysis on the sample prepared using high-concentration of Ag to further

verify this process. The result is shown in Figure S8 (Supporting Information). It was found that the peak intensity from the high-energy lattice plane of {001} significantly decrease when the Ag concentration is high in the AgPt bimetallic system. This condition may produce AgPt nanofern with lower surface reactivity.

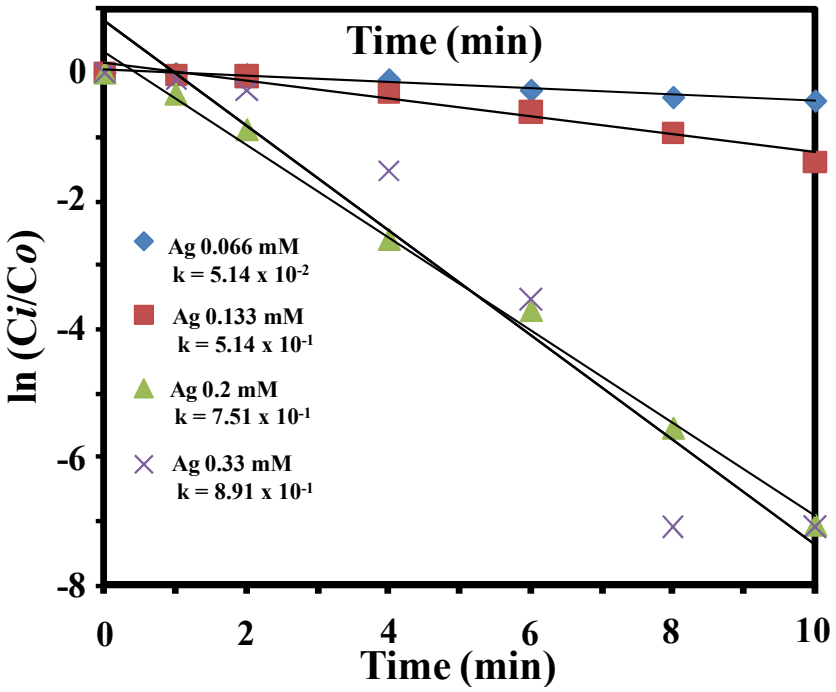

Figure 9. The photodegradation kinetic rate of MO over AgPt nanofern prepared at different Ag^{+} ions concentrations.

The extent of solar light irradiation to the MO degradation was examined to verify the photocatalytic efficiency of the AgPt nanofern. A reaction time as long as 100 min was taken in this study. It was found that no observable degradation was obtained, indicating the contribution of light irradiation to the MO degradation can be simply neglected (see Figure S9, Supporting Information).

It is true that the temperature programmed desorption (TPD) and temperature programmed reduction (TPR) of hydrogen are required to determine the active sites on the

catalyst surface. Unfortunately, due to the catalyst system is on the substrate surface of which is their amount is very small on the substrate surface, below the minimum resolution of the machine, the result cannot be obtained. Therefore, the active site was approximately determined by the BET surface analysis result. The TON and TOF values of the AgPt nanofern could probably be more higher if the exact hydrogen-desorption or hydrogen reduction behavior obtained from the TPD or TPR analysis due to specific feature of chemisorption process that merely depends on the accessible active sites, instead of available surface area. Nevertheless, the effort to obtain detailed surface reactivity of the AgPt nanofern is being pursued.

While the photocatalytic degradation of MO over the metaloxide catalysts, such as TiO_2, ZnO, etc., are known to be via either the hole scavenging (at high MO concentration) or hydroxyl oxidation (at low MO concentration) processes [45], the mechanism of the MO degradation in the presence process is still not yet clearly understood. However, we assume the degradation reaction can be more or less via similar process to that of photodegradation using metaloxide catalyst. It is well-known that during the photodegradation of organic dye, many active species can be produced, such as hydroxyl radicals ($^{\bullet}OH$), superoxide radicals ($^{\bullet}O_2^-$), electrons (e^-) and holes (h^+) [46]. As has been mentioned at the beginning, depending on the dye concentration, some process may be dominant while others dampened. For the present system using bimetallic system of AgPt, the role of h^+ active species can be neglected as no electronic excitation during the light irradiation in the bimetallic system[47]. Therefore, we assume that the rest active species, namely hydroxyl radical, superoxide radicals and electron may have some role in the reaction. However, in most catalytic degradation reaction of MO, hydroxyl oxidation is prevailing. By considering the structure and the properties of AgPt nanofern, similar phenomenon should be occurred. This process involves the adsorption of water molecules onto the AgPt nanofern surface and then dissociation to form $^{\bullet}OH$ by the high-energy surface of catalyst. The $^{\bullet}OH$ will then oxidize the double bond of MO molecules for a MO degradation.

The effective charge-transfer process between photo-excited-MO and the AgPt catalyst via "electron scavenging" like process by the nanocatalyst can also be considered for the photodegradation of MO. It has been well-known that the AgPt nanostructure features highly oxidizing properties due to having half-filled Pt f orbital that may attack the π bond in the MO

molecule. Prior to the oxidizing process the MO might be adsorbed onto the surface of AgPt nanofern surface[29]. During the UV light irradiation the π electron will excite, increasing the potential energy of the MO that in turn causes the molecule unstable enough to resist electron scavenging (oxidation) by the AgPt nanofern catalyst. The charge transfer does not occur in the absence of light irradiation (see Figure S8, Supporting Information for catalytic property study of AgPt nanofern in the absence of light source). Considering the concentration of MO used in this study was relatively low, i.e. approximately 6×10^{-5} M, one may think the hydroxyl oxidation might be the dominant process for MO degradation. However, by taking into account the formation of OH radical on the surface of AgPt catalyst might be limited due to possible active charge-transfer between free-electron of AgPt high-energy lattice plane and the excited state MO, the first process might be dampened, making the second mechanism (i.e. charge-transfer or electron scavenging)[47, 48] is the most appropriate method for MO degradation in this study.

Further study on the role of active species involved in the degradation of MO, such as via electron paramagnetic resonance (EPR), electron spin resonance (ESR) or liquid-column mass-spectrometry (LC-MS), is required to obtain exact mechanism underlying the MO photodegradation in the present study[49-51]. Unfortunately, due to limited availability of the apparatus, the result cannot be obtained at this moment. It is true that a straightforward chemical method is also possible to understand the physics and chemistry behind the photodegradation of MO, namely by using isoprophyl alcohol, benzoquinone and EDTA as hydroxyl, superoxide and hole scavengers[46], respectively. However, because of the present AgPt nanofern feature a highly-active surface property that facilitates rapid surface reaction, the use of chemical method is predicted to generate additional issues involving the catalyst surface-scavenger interaction. Nevertheless, the attempt to understand the mechanism behind the photocatalytic degradation of MO over the AgPt nanofern catalyst is being pursued and the result will be reported separately.

4. Conclusions

Synthesis of AgPt nanofern directly on the substrate surface has been demonstrated. The nanofern is composed by square-based nanopyramidal structures that oriented each other via

surface energy minimalisation. According to the HRTEM analysis, the nanopyramid that composed the nanofern possess four (001) high-energy plane of fcc with sharp spikes and vertices. The AgPt nanofern promises highly efficient catalytic properties due to their high-energy structure with (001) faces, sharp-spikes and –vertices and highly-surface defect. Heterogeneous photocatalytic properties of AgPt nanofern was evaluated in the degradation of methyl orange (MO). In typical process, it was found that the 20 ppm of MO can be almost completely degraded within the reaction time as short as 8 min using only single ITO substrate containing AgPt nanofern. The kinetic degradation analysis found that the ToF of the reaction is as high as 154 min^{-1}, which is relatively high in the viewpoint of heterogeneous photocatalysis. High-density of high-energy sites on the AgPt nanofern is considered as the key factor for the high catalytic performance of the AgPt nanofern. The present new nanostructure may find potential used in organic reaction and electrochemical applications.

Acknowledgement

The authors would like to acknowledge Universiti Kebangsaan Malaysia and Ministry of Higher Education (MOHE), Malaysia for funding this work under research grants DIP-2012-16 and FRGS/1/2013/SG02/UKM/02/8 and HiCOE Project. The authors are also grateful for the financial support received from Ministry of Science, Technology and Innovation (MOSTI), Malaysia for the funding under Science Fund grant (06-01-02-SF1157).

References

1. K. V. Luzyanin, A. G. Tskhovrebov, M. C. Carias, M. F. t. C. Guedes da Silva, A. J. L. Pombeiro and V. Y. Kukushkin, *Organometallics*, 2009, **28**, 6559-6566.
2. S. Mandal, D. Roy, R. V. Chaudhari and M. Sastry, *Chem Mater*, 2004, **16**, 3714-3724.
3. A. I. Tripolskii, N. V. Pavlenko, G. M. Talbiz and G. I. Golodets, *React Kinet Catal L*, 1983, **22**, 367-370.
4. L. N. Lewis and N. Lewis, *J Am Chem Soc*, 1986, **108**, 7228-7231.
5. A. Balouch, A. A. Umar, S. T. Tan, S. Nafisah, S. K. Md Saad, M. M. Salleh and M. Oyama, *Rsc Adv*, 2013, **3**, 19789-19792.
6. P. B. Kettler, *Organic Process Research & Development*, 2003, **7**, 342-354.
7. A. Demortiere, P. Launois, N. Goubet, P. A. Albouy and C. Petit, *J Phys Chem B*, 2008, **112**, 14583-14592.
8. R. Ferrando, J. Jellinek and R. L. Johnston, *Chemical Reviews*, 2008, **108**, 845-910.

9. J. Xu, T. Zhao, W. Yang and S. Shen, *international journal of hydrogen energy*, 2010, **35**, 8699-8706.
10. M. Kotobuki, A. Watanabe, H. Uchida, H. Yamashita and M. Watanabe, *Applied Catalysis A: General*, 2006, **307**, 275-283.
11. M. A. Rigsby, W.-P. Zhou, A. Lewera, H. T. Duong, P. S. Bagus, W. Jaegermann, R. Hunger and A. Wieckowski, *The Journal of Physical Chemistry C*, 2008, **112**, 15595-15601.
12. Y.-W. Lee, A.-R. Ko, S.-B. Han, H.-S. Kim and K.-W. Park, *Physical Chemistry Chemical Physics*, 2011, **13**, 5569-5572.
13. K.-W. Park, J.-H. Choi and Y.-E. Sung, *The Journal of Physical Chemistry B*, 2003, **107**, 5851-5856.
14. J.-H. Choi, K.-W. Park, I.-S. Park, W.-H. Nam and Y.-E. Sung, *Electrochimica acta*, 2004, **50**, 787-790.
15. J. Xu, T. Zhao and Z. Liang, *The Journal of Physical Chemistry C*, 2008, **112**, 17362-17367.
16. W. He, X. Wu, J. Liu, K. Zhang, W. Chu, L. Feng, X. Hu, W. Zhou and S. Xie, *The Journal of Physical Chemistry C*, 2009, **113**, 10505-10510.
17. H. You, Z. Peng, J. Wu and H. Yang, *Chem Commun*, 2011, **47**, 12595-12597.
18. L. C. Jones and M. J. Gordon, *The Journal of Physical Chemistry C*, 2012, **116**, 23472-23476.
19. M. T. Schaal, M. P. Hyman, M. Rangan, S. Ma, C. T. Williams, J. R. Monnier and J. W. Medlin, *Surf Sci*, 2009, **603**, 690-696.
20. J. A. Rodriguez and M. Kuhn, *The Journal of Physical Chemistry*, 1994, **98**, 11251-11255.
21. Z. Peng and H. Yang, *J Solid State Chem*, 2008, **181**, 1546-1551.
22. Z. Peng, H. You and H. Yang, *Advanced Functional Materials*, 2010, **20**, 3734-3741.
23. B. Gilbert, F. Huang, H. Zhang, G. A. Waychunas and J. F. Banfield, *Science*, 2004, **305**, 651-654.
24. J. M. Yuk, J. Park, P. Ercius, K. Kim, D. J. Hellebusch, M. F. Crommie, J. Y. Lee, A. Zettl and A. P. Alivisatos, *Science*, 2012, **336**, 61-64.
25. J. F. Banfield, S. A. Welch, H. Zhang, T. T. Ebert and R. L. Penn, *Science*, 2000, **289**, 751-754.
26. W. Zhang, J. Yang and X. Lu, *Acs Nano*, 2012, **6**, 7397-7405.
27. D. Li, M. H. Nielsen, J. R. I. Lee, C. Frandsen, J. F. Banfield and J. J. De Yoreo, *Science*, 2012, **336**, 1014-1018.
28. A. Balouch, A. Ali Umar, A. A. Shah, M. Mat Salleh and M. Oyama, *ACS Applied Materials and Interfaces*, 2013, **5**, 9843-9849.
29. G. Swiegers, in *Mechanical Catalysis*, John Wiley & Sons, Inc., 2008, pp. 337-339.
30. S. Kozuch and J. M. L. Martin, *ACS Catalysis*, 2012, **2**, 2787-2794.
31. C. H. Bartholomew, *Applied Catalysis A: General*, 2001, **212**, 17-60.
32. S. Kozuch and S. Shaik, *The Journal of Physical Chemistry A*, 2008, **112**, 6032-6041.
33. X. Wei, X.-F. Yang, A.-Q. Wang, L. Li, X.-Y. Liu, T. Zhang, C.-Y. Mou and J. Li, *The Journal of Physical Chemistry C*, 2012, **116**, 6222-6232.
34. E. B. Maxted, in *Advances in Catalysis*, eds. V. I. K. E. K. R. P. H. E. W.G. Frankenburg and H. S. Taylor, Academic Press, 1951, pp. 129-178.

35. C. T. Campbell, *Accounts Chem Res*, 2013, **46**, 1712-1719.
36. R. P. H. Gasser and P. R. Vaight, *Nature*, 1970, **225**, 933-936.
37. Y. Zhao, J. Chu, S.-H. Li, Y. Chen, G.-P. Sheng, Y.-P. Chen, W.-W. Li, G. Liu, Y.-C. Tian, Y. Xiong and H.-Q. Yu, *Chem Eng J*, 2011, **170**, 440-444.
38. N. Zhang, S. Liu, X. Fu and Y.-J. Xu, *The Journal of Physical Chemistry C*, 2011, **115**, 9136-9145.
39. J. Fang, F. Shi, J. Bu, J. Ding, S. Xu, J. Bao, Y. Ma, Z. Jiang, W. Zhang, C. Gao and W. Huang, *The Journal of Physical Chemistry C*, 2010, **114**, 7940-7948.
40. T. Chen, Y. Zheng, J.-M. Lin and G. Chen, *Journal of the American Society for Mass Spectrometry*, 2008, **19**, 997-1003.
41. A. T. Kuvarega, R. W. M. Krause and B. B. Mamba, *The Journal of Physical Chemistry C*, 2011, **115**, 22110-22120.
42. B. Wang, S. Yin, G. Wang, A. Buldum and J. Zhao, *Phys Rev Lett*, 2001, **86**, 2046-2049.
43. J. Weissmüller, R. N. Viswanath, D. Kramer, P. Zimmer, R. Würschum and H. Gleiter, *Science*, 2003, **300**, 312-315.
44. R. M. Wang, O. Dmitrieva, M. Farle, G. Dumpich, H. Q. Ye, H. Poppa, R. Kilaas and C. Kisielowski, *Phys Rev Lett*, 2008, **100**, 017205.
45. L. Yu, J. Xi, M.-D. Li, H. T. Chan, T. Su, D. L. Phillips and W. K. Chan, *Phys Chem Chem Phys*, 2012, **14**, 3589-3595.
46. W. J. Kim, D. Pradhan, B.-K. Min and Y. Sohn, *Applied Catalysis B: Environmental*, 2014, **147**, 711-725.
47. M. A. Mahmoud, D. O'Neil and M. A. El-Sayed, *Chem Mater*, 2013, **26**, 44-58.
48. A. Wittstock, A. Wichmann and M. Bäumer, *ACS Catalysis*, 2012, **2**, 2199-2215.
49. Y. Chen, D. Li, X. Wang, L. Wu, X. Wang and X. Fu, *New J Chem*, 2005, **29**, 1514-1519.
50. M. Yin, Z. Li, J. Kou and Z. Zou, *Environ Sci Technol*, 2009, **43**, 8361-8366.
51. J. Xu, W. Meng, Y. Zhang, L. Li and C. Guo, *Applied Catalysis B: Environmental*, 2011, **107**, 355-362.

Graphical abstract

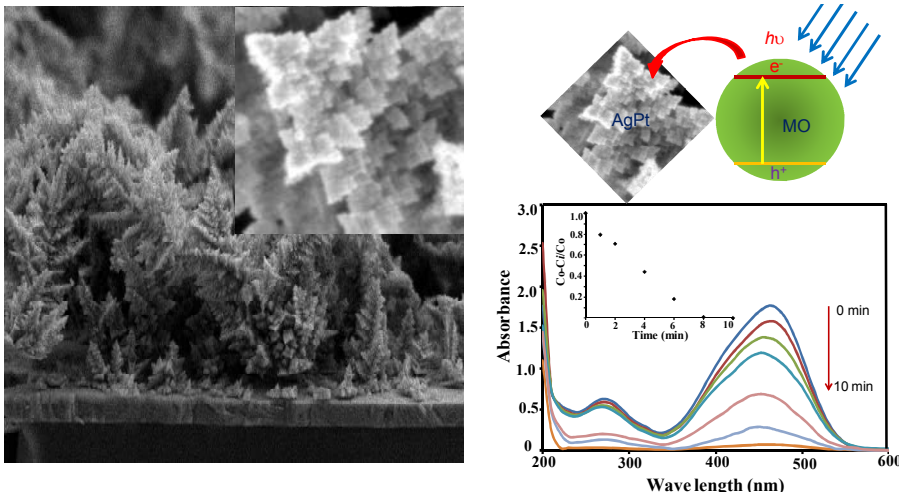

A straightforward approach to synthesize novel nanopyramidal spike composed nanofern of AgPt bimetals vertically-oriented on the substrate is presented. The nanostructures are characterized by rich {001} high-energy lattice plane of fcc system. The AgPt bimetal system shows excellent heterogeneous photocatalytic performance in the degradation of methylene orange.